

Dimensional Accuracy of 17-4 PH SS Geometric Features Fabricated Using L-PBF and MBJ Technologies

Indrajit Nandi^{1,2}, Quentin Charron³, Paul R. Gradl⁴, Guillaume Mohara³, Benoit Verquin³, Shuai Shao^{1,2}, Nima Shamsaei^{1,2*}

¹ National Center for Additive Manufacturing Excellence (NCAME), Auburn University, Auburn, AL 36849, USA

² Department of Mechanical Engineering, Auburn University, Auburn, AL 36849, USA

³ CETIM, 60304 Senlis, France

⁴ NASA Marshall Space Flight Center, Propulsion Department, Huntsville, AL 35812, USA

*Corresponding author: shamsaei@auburn.edu

Phone: (334) 844-4839

Abstract

This study investigates the dimensional tolerances of part fabricated by two metal additive manufacturing (AM) technologies, i.e., laser powder bed fusion (L-PBF) and metal binder jetting (MBJ), by fabricating a geometric feature build plate. The geometric feature build plate integrates standard ISO/ASTM test artifact geometries that include, but are not limited to, horizontal holes, varying angled walls, vertical features incorporating concentric hollow cylinders, protruding cylinders, etc. All the parts in the feature build plate were kept the same between L-PBF and MBJ technologies. Optical and mechanical measurement methods were employed on selected features in the build plate. The obtained results were analyzed for different features and compared between the two technologies. The difficulties experienced during the feature build plate fabrication are discussed in detail for both processes, and suggestions are made regarding strategies to overcome them.

Keywords: Additive manufacturing; 17-4 PH SS; Laser powder bed fusion (L-PBF); Metal binder jetting (MBJ); Feature build plate

Introduction

Metal additive manufacturing (AM) has gained interest in industries such as aerospace, automotive, biomedical, and energy due to its ability to produce complex, near-net-shaped parts directly from CAD models [1,2]. Unlike traditional subtractive methods, AM enables a bottom-up, layer-by-layer fabrication process that offers cost and design advantages, particularly for geometrically intricate components [3–5]. Among different AM technologies, laser powder bed fusion (L-PBF) is popular owing to its ability to fabricate parts with fine features [6–8]. Metal binder jetting (MBJ) is getting attention due to its ability to fabricate parts with high build rates [9,10].

L-PBF employs a focused laser to selectively melt metal powders in an inert environment, in a layer by layer manner until the fabrication is complete. However, L-PBF faces challenges such as process induced volumetric defect, heterogeneous microstructure, and residual stresses [11–14]. This can lead to a variation in the dimensional accuracy of the part fabricated by L-PBF and necessitate an investigation into its ability to fabricate complex parts with fine tolerances [15,16].

In contrast, MBJ fabricates parts without melting by using a polymer binder to bond powder particles layer by layer [17,18]. The printed "green" parts are later sintered to improve part density. MBJ offers advantages such as lower residual stress, better powder reusability, and the ability to fabricate larger parts with fewer support structures [19,20]. However, it faces limitations, including shrinkage and cracking of parts during sintering, and lower part density [21]. This often poses challenges in maintaining the dimensional tolerances of the fabricated parts [22].

Proper geometric dimensioning and tolerancing are requirements for integrating additively manufactured parts in industries. A part fabricated successfully in one AM technology can face challenges when fabricated using another, which can lead to variations in its dimensional accuracy. This highlights the importance of evaluating the dimensional accuracy of parts fabricated using different AM technologies. This study investigated the dimensional accuracy of a 17-4 precipitation hardened (PH) stainless steel (SS) feature build plate fabricated via L-PBF and MBJ. Challenges encountered and lessons learned during the fabrication are discussed, in addition to comparing the dimensional accuracy of parts in the feature build plate.

Experimental procedures

In this study, a feature build plate was adopted from a prior study to evaluate the dimensional accuracy of parts fabricated using L-PBF and MBJ [8]. The particle size distribution of 17-4 PH SS powder used for L-PBF was 15-53 μm and 6-53 μm for the MBJ. For MBJ, the feature build plate was fabricated using a Desktop Metal "SHOP System" suite, and for L-PBF, the same was fabricated using an EOS M290 machine using the manufacturer's recommended process parameters (see Table 1).

Table 1. Process parameters for the fabrication using L-PBF and MBJ.

L-PBF process parameters							
Machine model type	Layer height (μm)	Recoater type	Power (W)	Scan speed (mm/s)	Energy density (J/mm^3)	Core scan strategy	Shielding gas
EOS M290	40	Steel	285	960	74.2	Stripes	Ar
MBJ process parameters							
Printer	Layer height (μm)	Recoater type	Powder mix	Overflow ratio	Furnace	Sintering gas	
Desktop Metal “SHOP System”	75	Steel	90% recycled + 10% new	210%	Desktop Metal “STUDIO System”	Ar + 2% H_2	

The build layout (see Figure 1a), plate orientation during fabrication in L-PBF (see Figure 1b) and MBJ (see Figure 1c), and the fabricated plates (see Figure 1d & e) are presented. The feature build plate was fabricated successfully without any cracking or noticeable distortion of the parts in L-PBF. For MBJ, the majority of parts were fabricated without any distortion except for a few. Multiple long cracks were observed in the base plate, which was also part of the print in MBJ, unlike L-PBF, where the feature build plate was printed onto a steel base. However, the plate was intact and not cracked entirely. Multiple prints were needed, and modifications were implemented in the process parameters for the fabrication of this build plate in MBJ.

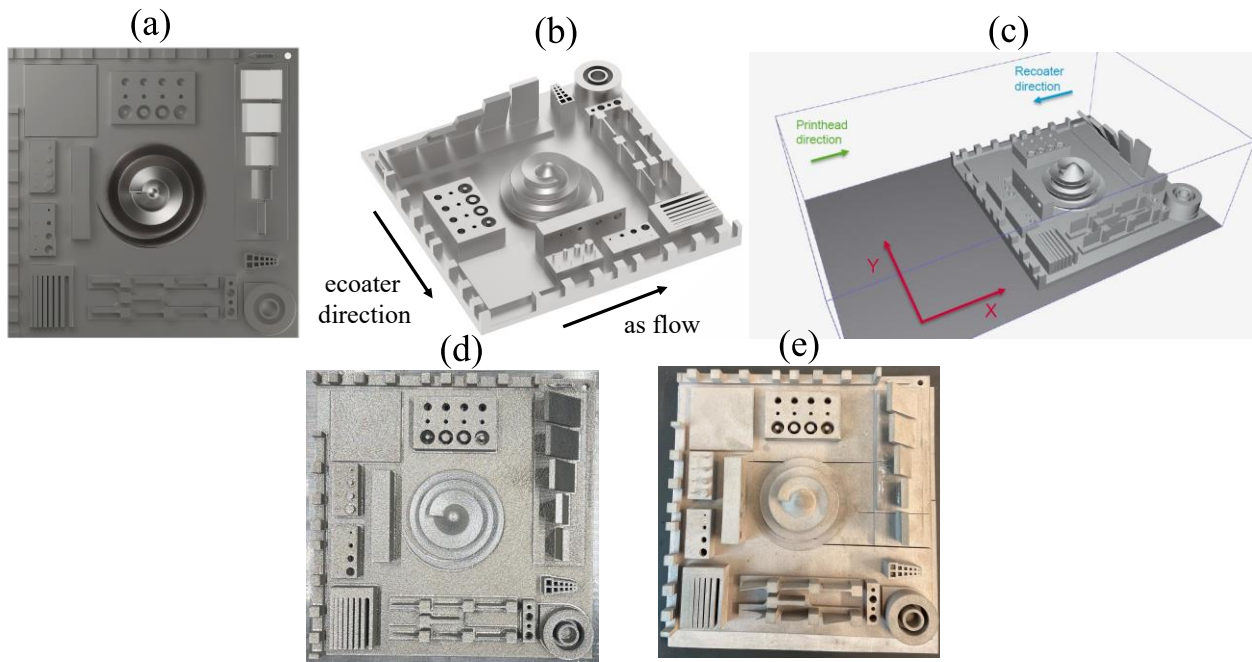


Figure 1. (a) Top view of the feature build plate design; recoater and gas flow directions for the (b) L-PBF and recoater and printhead direction for the (c) MBJ print. Fabricated (d) L-PBF and (e) MBJ feature build plates.

The feature build plate is 140 mm in the X-direction, 140 mm in the Y-direction, and 31.8 mm in the Z-direction. The designed volume of the plate is 143 cm³ with a total surface area of 722 cm² [8]. Geometric features in the build plate adhere to the ISO/ASTM 52902.2019 standards for test artifacts (see Figure 2) [23]. The features and architecture were designed such that they could be accessed without sectioning for line-of-sight 3D scanning. In addition, features were strategically positioned to minimize the impact of any potential failure on areas aligned with the recoater.

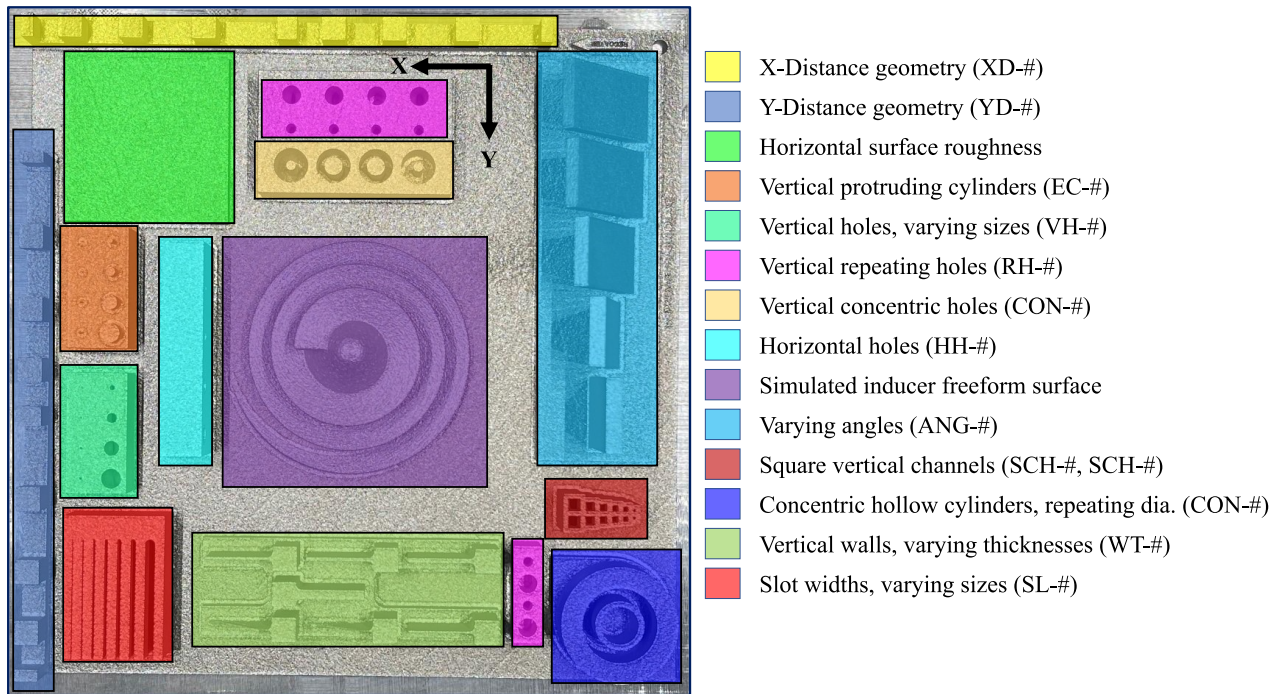


Figure 2. Feature build plate design with test artifacts shown on a L-PBF printed plate. Selected features from the plate were investigated in this current study.

Following the fabrication of the L-PBF and MBJ feature build plates, both were visually inspected and scanned for dimensional measurements using a GOM ATOS III-Triple Scan 8 M (Rev.02) structured light scanner with blue light fringe pattern projection similar to a previous study [8]. To minimize the diagnostic uncertainty and assure consistency, all scans were performed by a single operator.

Results and discussion

The major objective of this study was oriented towards investigating the fabricability of identical features and their dimensional accuracy using L-PBF and MBJ. Since the feature build plate was originally designed for L-PBF, some features were not adapted for MBJ. Thus, modification was made to successfully fabricate the feature build plate in MBJ.

A first production attempt in MBJ was made with a standard 17-4PH SS printing and sintering recipe (see Table 1), with no design modifications on the feature build plate (see Figure 3a). The green feature build plate showed several small cracks on the part up-skin (X-axis oriented, non-traversing) following the depowdering step (see Figure 3b).

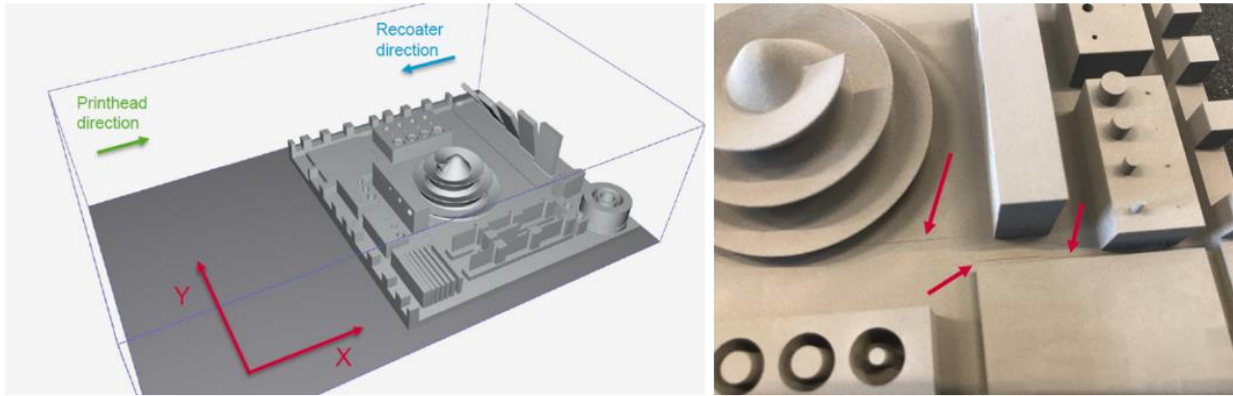


Figure 3 (a) Position of the feature build plate in the build area of the Shop printer, (b) Superficial cracks on the X-axis after curing and depowdering.

Upon depowdering, the feature build plate was sintered on a Desktop Metal furnace. Tearing on the feature build plate was observed post-sintering and attributed to an amplification of the cracks seen in the depowdering step (same position), as shown in Figure 4. Among the features on the build plate, significant sagging was observed on the angled walls. This was attributed to the absence of support for the angled walls during sintering. Some fine features, such as the thinner walls and several small pins, were broken in the depowdering step. This was due to the delicate features and green condition of the part during depowdering (use of brushes and blown air) and is not a printing limitation. Distortions on several features, such as thin walls and slot width, were observed as well.

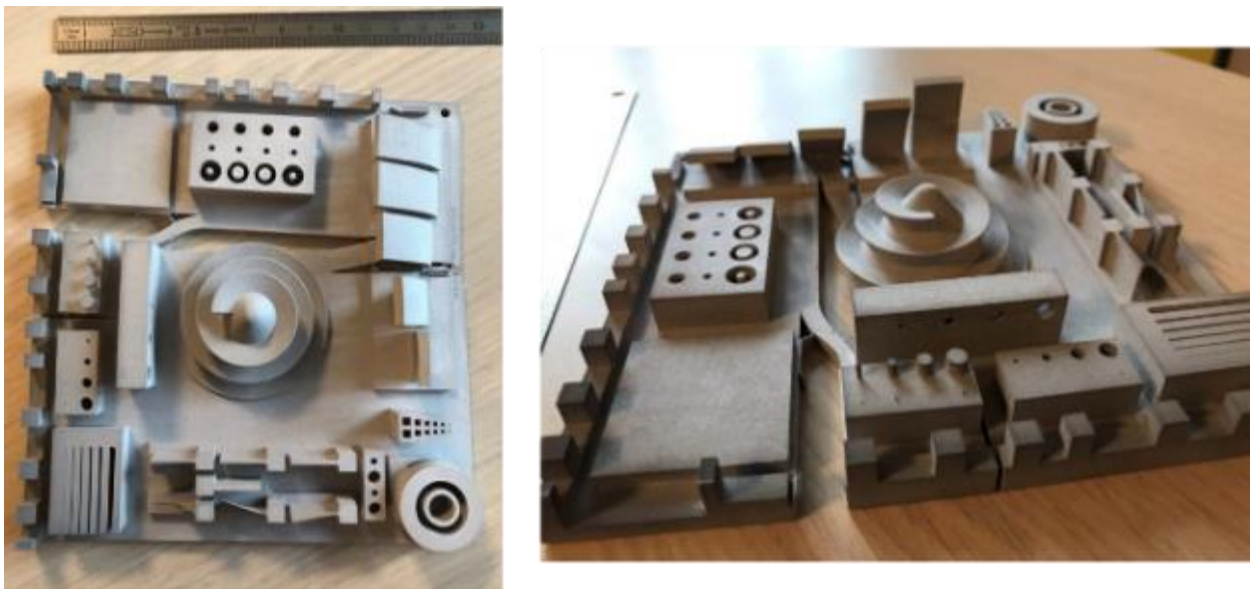


Figure 4. Post-sintering feature build plate with tearing localized on the observed cracks.

Following these results, a second iteration of the plate was done with several process adjustments to the printer and the feature build plate design. The modifications included deactivation of the bleed correction to favor the integrity of the fine features. Curing cycle ramp-up increased from 8h to 16h to provide even heating of the plate and mitigate crack formation. A global sintering support underneath the plate was used. The aim of this sacrificial support was to reduce any tearing by applying the friction force that occurs during shrinking to the sintering setter instead of on the part itself. In addition, support was provided to the previously sagged angled walls, except for the 90° wall. Ceramic powder coating was applied to the supports to avoid bonding between the part and the support itself, and then placed below the plate or underneath the angled walls.

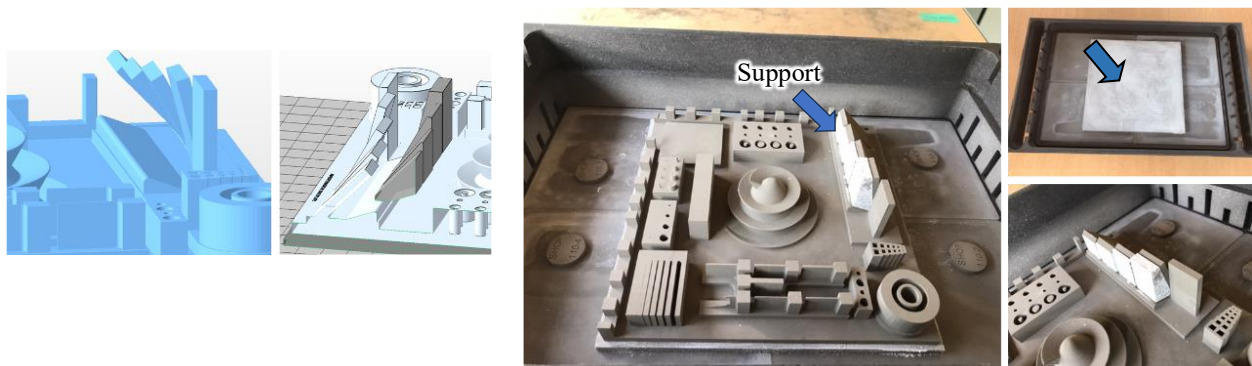


Figure 5. (a) Plate design modification for the implementation of sintering supports (grey blocks) and (b) Second feature build plate before sintering, supports in white (ceramic coated).

However, cracks appeared after curing and depowdering of the second iteration, which evolved into tearing upon sintering the plate, as shown in Figure 6. Although tearing was seen, several improvements were noted in the plate's quality. The curing adjustment did not have any visible effect on the small cracks, but the global support minimized the tearing during sintering. More intact fine features were produced, benefiting from both the deactivated bleed correction and the carefulness of the operator. The use of external support resulted in straighter angled walls. Residual powder pockets were avoided with additional controls after depowdering.

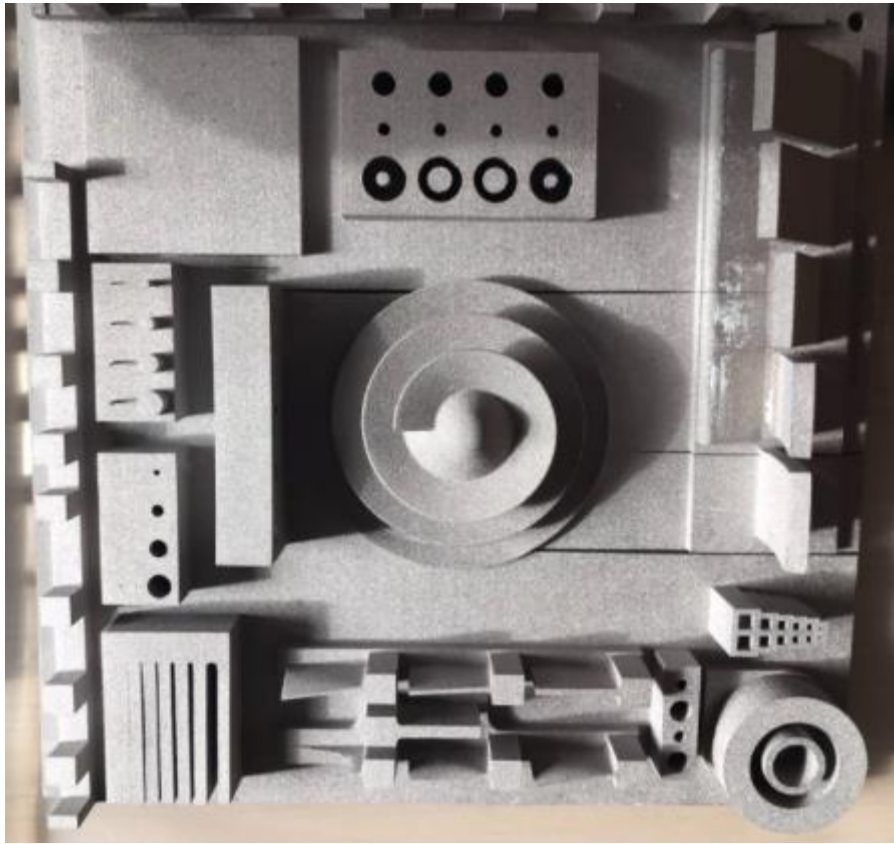


Figure 6. Second iteration post-sintering feature build plate with tearing localized on the observed cracks.

The cracks on the base plate were observed during both the first and second MBJ prints. It indicates a potential limitation of the MBJ technology in the production of large parts with high cross-sectional variation in the part design. It is likely that this combination led to the appearance of these cracks at the curing step of the process, which amplified into tearing upon sintering. The tearing of the plate and its global shrinkage during sintering may also have led to slumping and affected the accuracy of certain features, such as the slots.

The angled walls were originally designed for L-PBF, which showed sagging on the first MBJ build. Sagging is a common flaw found in MBJ, especially for tall features that tend to collapse under their own weight during sintering. The use of removable sintering supports mostly resolved the issue in the second iteration. However, the 90° angled wall, which remained unsupported during sintering, exhibited a deviation greater than 5° from its intended angle.

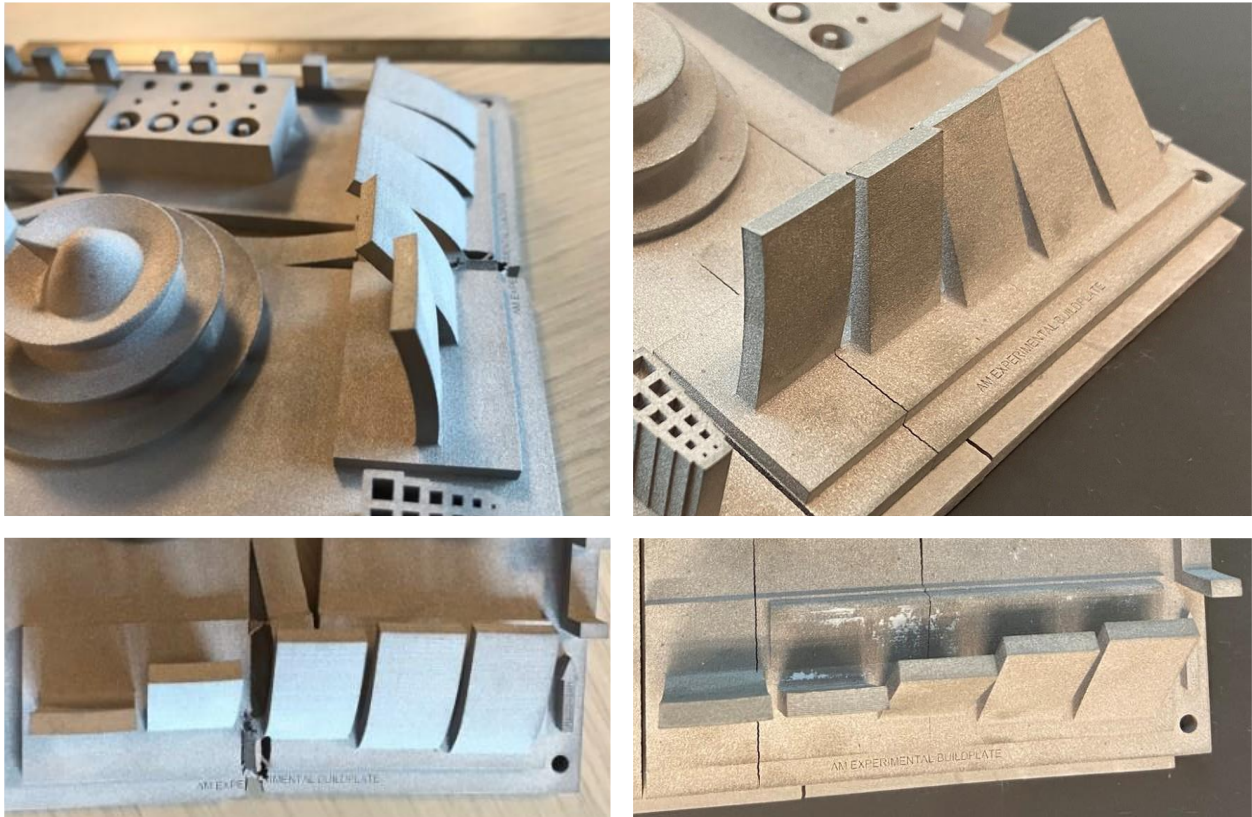


Figure 7. (a) Collapsed angled walls in the first production, (b) Angled walls from the second production with sintering support.

The measurements of the angled walls, i.e., ANG-1 to ANG-5 (90° , 75° , 60° , 50° , and 45°) on the L-PBF and MBJ feature build plates showed clear differences in part dimensions (see Figure 8). The highest deviation was observed for the 90° angled wall in the MBJ build plate, while 75° angled walls showed the lowest. This suggests that sintering support was needed for the 90° angled wall as well. The deviation from the design value increased for the 60° , 50° , and 45° angled walls. For L-PBF, the printed angled walls showed almost little to no deviation from their design values. The deviations observed in MBJ were attributed to the sagging effect seen on the walls during sintering, which was partially mitigated by the use of removable sintering supports.

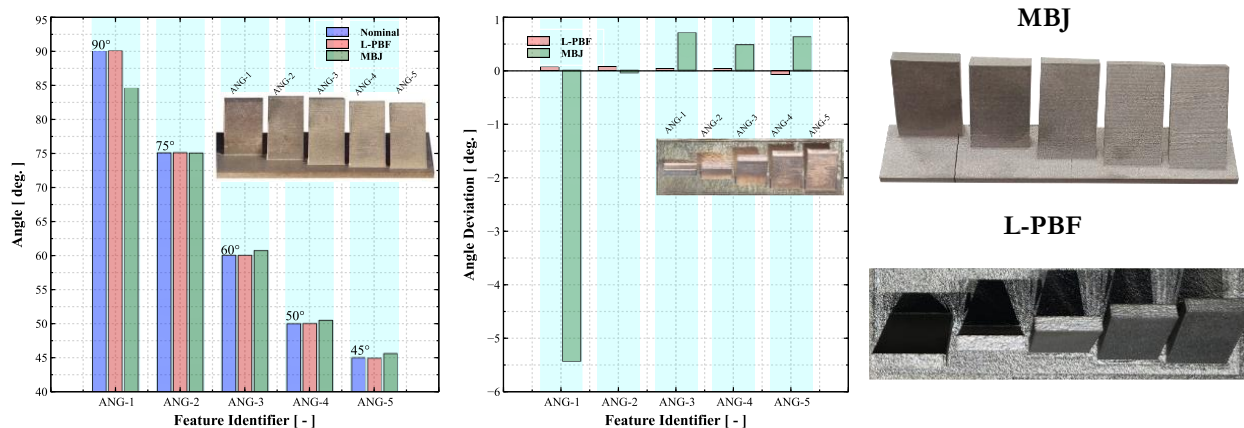


Figure 8. Dimensional accuracy of the angled walls between L-PBF and MBJ from their designed values.

To evaluate the part repeatability in L-PBF and MBJ technologies, three sets of 2.0 mm and 3.8 mm diameter vertical holes were printed at three different locations on the feature build plate. The diameter of the printed holes in MBJ was smaller than their design value, while for L-PBF, it was larger (see Figure 9). Among the two holes, the 2.00 mm hole showed higher deviation compared to the 3.8 mm hole in MBJ. This could be attributed to the powder residue left during the depowdering process in MBJ.

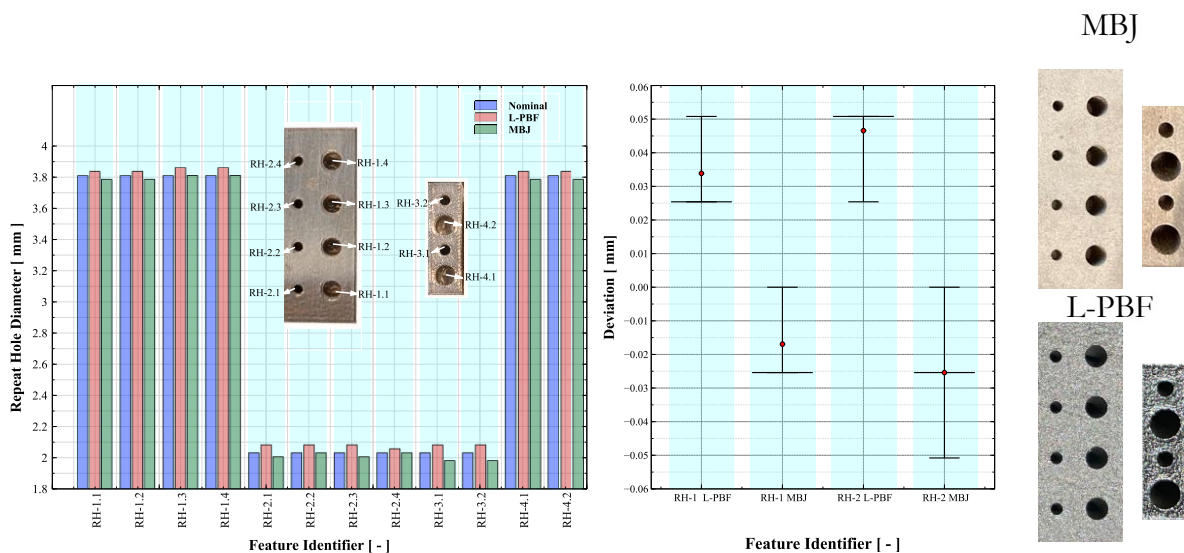


Figure 9. Evaluation of vertically repeated hole diameters showing differences in dimensional accuracy between L-PBF and MBJ from their designed values.

The measurements of the seven vertical walls with different thicknesses, i.e., WT-1 to WT-7 (0.10, 0.20, 0.41, 0.61, 0.81, 1.0, and 2.0 mm) on the L-PBF and MBJ feature build plates are shown in Figure 10. In the MBJ build, all walls were printed successfully except for the 0.10 mm wall, which was partially printed and considered a failure. Distortions were observed in the 0.20, 0.41, and 0.61 mm thick walls, which appeared during the sintering step. The breakage of

the 0.10 mm wall was attributed to the build plate handling in the depowdering step and not necessarily from a printer limitation. In L-PBF, the 0.10 and 0.20 mm walls were partially printed and considered as failed. The remaining walls (WT-4 to WT-7) were printed successfully, and no significant distortion was observed. The walls printed by the MBJ were thicker compared to their design values, while for L-PBF, they were thinner. The increase in wall thickness in MBJ was attributed to the excessive binder spreading during deposition, creating a bleeding effect. This effect was not compensated for in this print to ensure a stronger plate and maximize the survivability of other features on the feature build plate.

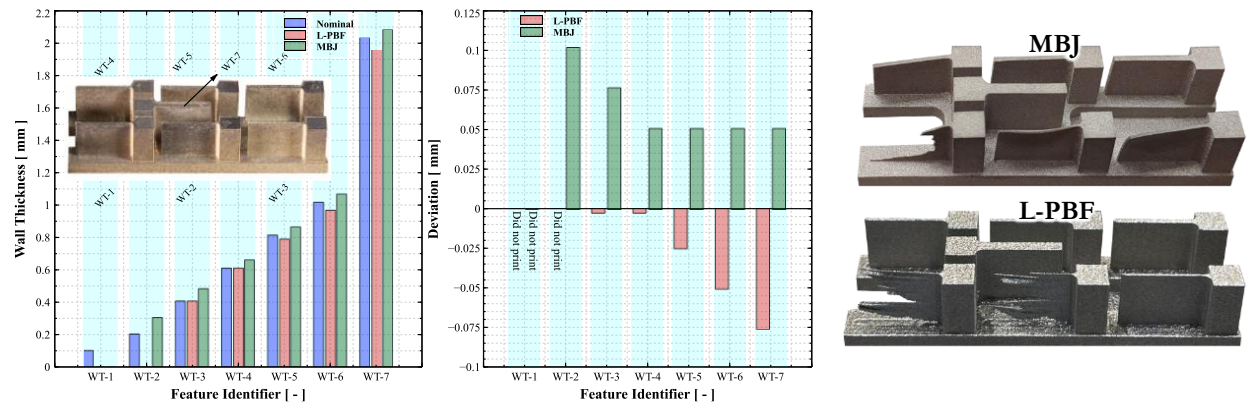


Figure 10. Evaluation of wall thickness: difference in the dimensional accuracy in L-PBF and MBJ from the designed value.

Conclusions

The objective of this study was to investigate the dimensional accuracy of geometric features across different AM technologies. A feature build plate, originally designed for the L-PBF, was fabricated using both L-PBF and MBJ. Multiple iterations and design modifications were required for a successful print using MBJ, and the lessons learned from the process were discussed. Based on the results, the following conclusions can be drawn:

1. MBJ showed lower dimensional accuracy for printing holes due to sintering shrinkage but showed better accuracy for solid parts. It indicated that MBJ can print solid parts with higher dimensional accuracy, but for holes, design modifications are needed due to the sintering shrinkage.
2. Angled walls require support when printing in MBJ to prevent sagging. L-PBF produced the same part with little to no deviation, showing better accuracy for unsupported features.
3. Walls at 0.20 mm and below thickness failed to print L-PBF, while only 0.10 mm walls failed for the MBJ. Thinner walls in MBJ showed higher deviation from their design values compared to L-PBF.
4. Fabricating a common feature build plate using both L-PBF and MBJ presented challenges in this study, suggesting that not all AM technologies suit every geometry. Evaluations are needed prior to selecting AM technology for part fabrication.

Acknowledgment

This study is partially supported by the National Aeronautics and Space Administration (NASA) under Cooperative Agreement No. 80MSFC19C0010. This paper describes objective technical results and analysis. Any subjective views or opinions that might be expressed in the paper do not necessarily represent the views of NASA or the United States Government.

References

- [1] Shamsaei N, Yadollahi A, Bian L, Thompson SM. An overview of Direct Laser Deposition for additive manufacturing; Part II: Mechanical behavior, process parameter optimization and control. *Addit Manuf* 2015;8:12–35. <https://doi.org/10.1016/J.ADDMA.2015.07.002>.
- [2] Thompson SM, Bian L, Shamsaei N, Yadollahi A. An overview of Direct Laser Deposition for additive manufacturing; Part I: Transport phenomena, modeling and diagnostics. *Addit Manuf* 2015;8:36–62. <https://doi.org/10.1016/J.ADDMA.2015.07.001>.
- [3] Blakey-Milner B, Gradl P, Snedden G, Brooks M, Pitot J, Lopez E, et al. Metal additive manufacturing in aerospace: A review. *Mater Des* 2021;209. <https://doi.org/10.1016/J.MATDES.2021.110008>.
- [4] Vafadar A, Guzzomi F, Rassau A, Hayward K. Advances in metal additive manufacturing: A review of common processes, industrial applications, and current challenges. *Applied Sciences (Switzerland)* 2021;11:1–33. <https://doi.org/10.3390/APP11031213>.
- [5] Chen Z, Han C, Gao M, Kandukuri SY, Zhou K. A review on qualification and certification for metal additive manufacturing. <https://doi.org/10.1080/17452759.2021.2018938> 2021;17:382–405. <https://doi.org/10.1080/17452759.2021.2018938>.
- [6] Herzog D, Seyda V, Wycisk E, Emmelmann C. Additive manufacturing of metals. *Acta Mater* 2016;117:371–92. <https://doi.org/10.1016/J.ACTAMAT.2016.07.019>.
- [7] Yeung H, Lane B, Fox J. Part geometry and conduction-based laser power control for powder bed fusion additive manufacturing. *Addit Manuf* 2019;30:100844. <https://doi.org/10.1016/J.ADDMA.2019.100844>.
- [8] Gradl PR, Tinker DC, Ivester J, Skinner SW, Teasley T, Bili JL. Geometric feature reproducibility for laser powder bed fusion (L-PBF) additive manufacturing with Inconel 718. *Addit Manuf* 2021;47:102305. <https://doi.org/10.1016/J.ADDMA.2021.102305>.
- [9] Sukhotskiy V, Pascall AJ, Jeffries JR, Livermore L. Enabling multi-resolution droplet-on-demand metal jetting through tailored pulsing. *Npj Advanced Manufacturing* 2025 2:1 2025;2:1–11. <https://doi.org/10.1038/s44334-025-00029-w>.
- [10] Hofmann U, Ferchow J, Meboldt M. Evaluating effect of manufacturing process on design in metal binder jetting. *Results in Engineering* 2024;24:103430. <https://doi.org/10.1016/J.RINENG.2024.103430>.

- [11] Brennan MC, Keist JS, Palmer TA, Bourell DL, Frazier W, Kuhn H, et al. Defects in Metal Additive Manufacturing Processes. *Journal of Materials Engineering and Performance* 2021 30:7 2021;30:4808–18. <https://doi.org/10.1007/S11665-021-05919-6>.
- [12] Mostafaei A, Zhao C, He Y, Reza Ghiaasiaan S, Shi B, Shao S, et al. Defects and anomalies in powder bed fusion metal additive manufacturing. *Curr Opin Solid State Mater Sci* 2022;26:100974. <https://doi.org/10.1016/J.COSSMS.2021.100974>.
- [13] Mugwagwa L, Yadroitsava I, Makoana NW, Yadroitsev I. Residual stress in laser powder bed fusion. *Fundamentals of Laser Powder Bed Fusion of Metals* 2021:245–76. <https://doi.org/10.1016/B978-0-12-824090-8.00014-7>.
- [14] Khan MF, Ghiaasiaan R, Gradl PR, Shao S, Shamsaei N. Additively Manufactured Scalmalloy via Laser Powder Bed Fusion (L-PBF): Temperature-Dependent Tensile and Fatigue Behaviors. *Fatigue Fract Eng Mater Struct* 2025;48:1496–513. <https://doi.org/10.1111/FFE.14549>.
- [15] Ameta G, Lipman R, Moylan S, Witherell P. Investigating the Role of Geometric Dimensioning and Tolerancing in Additive Manufacturing. *Journal of Mechanical Design, Transactions of the ASME* 2015;137. <https://doi.org/10.1115/1.4031296>.
- [16] Maleki E, Salehnasab B, Paul M, Shao S, Shamsaei N. Dimensional accuracy of fabricated geometries through powder bed fusion: An overview and a new benchmark artifact proposal. *Mater Des* 2025;257:114361. <https://doi.org/10.1016/J.MATDES.2025.114361>.
- [17] Ziaee M, Tridas EM, Crane NB. Binder-Jet Printing of Fine Stainless Steel Powder with Varied Final Density. *JOM* 2017;69:592–6. <https://doi.org/10.1007/S11837-016-2177-6>.
- [18] Li M, Du W, Elwany A, Pei Z, Ma C. Metal binder jetting additive manufacturing: A literature review. *Journal of Manufacturing Science and Engineering, Transactions of the ASME* 2020;142. <https://doi.org/10.1115/1.4047430/1084395>.
- [19] Bidare P, Abdullah R, Jiménez A, Essa K. Powder reusability in metal binder jetting. *Proceedings of the Institution of Mechanical Engineers Part E Journal of Process Mechanical Engineering* 2023;238:1554–60. <https://doi.org/10.1177/09544089221147778>.
- [20] Blunk H, Seibel A. Design guidelines for metal binder jetting. *Progress in Additive Manufacturing* 2024;9:725–32. <https://doi.org/10.1007/S40964-023-00475-Y/TABLES/3>.
- [21] Chen Z, Wan B, Liu J, Zhu D, Wang H, Chen W, et al. Sintering densification mechanism of binder jet 3D printing 316L stainless steel parts via dimensional compensation technology. *Journal of Materials Research and Technology* 2024;33:3296–307. <https://doi.org/10.1016/J.JMRT.2024.10.041>.
- [22] Oh JW, Nahm S, Kim B, Choi H. Anisotropy in green body bending strength due to additive direction in the binder-jetting additive manufacturing process. *Journal of Korean Institute of Metals and Materials* 2019;57:227–35. <https://doi.org/10.3365/KJMM.2019.57.4.227>.
- [23] ISO/ASTM 52902:2019 - Additive manufacturing — Test artifacts — Geometric capability assessment of additive manufacturing systems n.d. <https://www.iso.org/standard/67287.html> (accessed June 19, 2025).